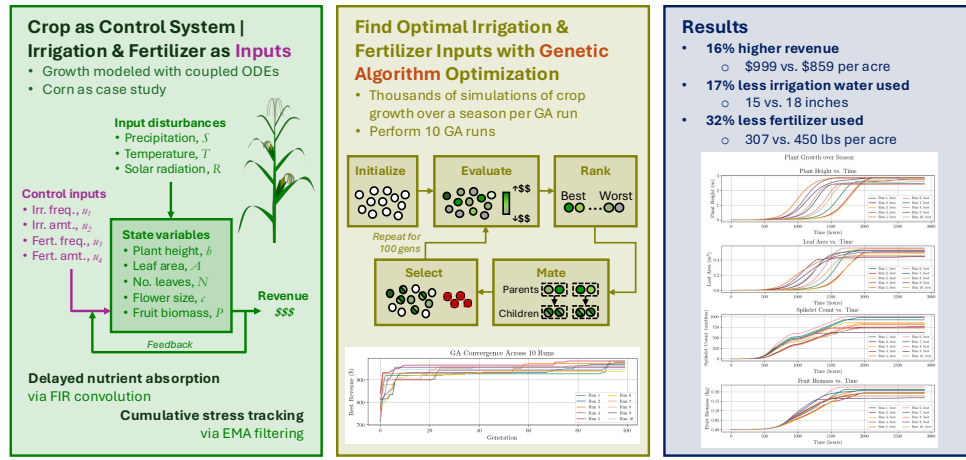


# 1 Graphical Abstract

## 2 Optimizing irrigation and fertilizer strategy using a crop growth model with delayed nutrient absorption dynamics

4 Carla J. Becker, Tarek I. Zohdi

### Optimizing Irrigation & Fertilizer Strategy via Crop Model + Genetic Algorithm



UC Berkeley Carla J. Becker, Tarek I. Zohdi (2026)

5    Highlights

6    **Optimizing irrigation and fertilizer strategy using a crop growth**  
7    **model with delayed nutrient absorption dynamics**

8    Carla J. Becker, Tarek I. Zohdi

- 9       • Reduced-order coupled ODE model; efficient alternative to DSSAT/AP-  
10      SIM
- 11      • FIR convolution formulation for delayed nutrient absorption dynamics
- 12      • EMA filtering for cumulative environmental stress tracking
- 13      • GA optimization of irrigation/fertilization schedules to maximize rev-  
14      enue
- 15      • Calibration and validation against Iowa corn agronomic data

16 Optimizing irrigation and fertilizer strategy using a crop  
17 growth model with delayed nutrient absorption  
18 dynamics

19 Carla J. Becker, Tarek I. Zohdi

<sup>a</sup>*Department of Mechanical Engineering, University of California, Berkeley, 6141  
Etcheverry Hall, Berkeley, 94720, California, United States of America*

<sup>b</sup>*Department of Mechanical Engineering, University of California, Berkeley, 6141  
Etcheverry Hall, Berkeley, 94720, California, United States of America*

---

20 **Abstract**

21 **CONTEXT** Rising production costs and declining commodity prices have  
22 motivated farmers to seek computational tools for optimizing resource appli-  
23 cation. While sophisticated crop models such as DSSAT and APSIM simulate  
24 detailed physiological processes, they require extensive parameterization and  
25 may be computationally expensive for optimization applications. Moreover,  
26 existing optimization approaches often use simplified plant response models  
27 that do not capture the delayed, cumulative effects of resource application.

28  
29 **OBJECTIVE** This study develops a reduced-order crop growth model that  
30 captures delayed nutrient absorption dynamics and couples it with a genetic  
31 algorithm to optimize irrigation and fertilizer strategies that maximize net  
32 revenue while minimizing input costs.

33  
34 **METHODS** We present a generalized, coupled ordinary differential equa-  
35 tion (ODE) model tracking five state variables—plant height, leaf area, num-  
36 ber of leaves, flower size, and fruit biomass—each governed by logistic growth  
37 with time-varying growth rates and carrying capacities. These parameters  
38 are modulated by nutrient factors quantifying how well actual water, fertil-  
39 izer, temperature, and solar radiation levels match expected values. Delayed  
40 physiological response is captured using finite impulse response (FIR) con-  
41 volution with Gaussian kernels, where different temporal spreads represent  
42 distinct metabolic timescales for each input type. Cumulative stress from sus-  
43 tained deviations is tracked using exponential moving average (EMA) filters.

<sup>44</sup> A genetic algorithm searches over application frequency and amount for both  
<sup>45</sup> irrigation and fertilizer, evaluating candidate strategies through full-season  
<sup>46</sup> simulations. The framework is demonstrated using corn grown in Fairfax,  
<sup>47</sup> Iowa, with historical weather data under a drought scenario (50% of typical  
<sup>48</sup> precipitation).

<sup>49</sup>

<sup>50</sup> **RESULTS AND CONCLUSIONS** The genetic algorithm identifies non-  
<sup>51</sup> intuitive strategies that outperform conventional uniform application sched-  
<sup>52</sup> ules, achieving 16% higher net revenue (\$999 vs. \$859 per acre) through  
<sup>53</sup> strategic timing of resource inputs. The optimized strategies use 17% less ir-  
<sup>54</sup> rigation (15 vs. 18 inches) and 32% less fertilizer (307 vs. 450 lbs) than farmer  
<sup>55</sup> best practices while achieving comparable or higher crop yields. Across 10  
<sup>56</sup> independent optimization runs, 9 outperformed the baseline, demonstrating  
<sup>57</sup> algorithm robustness.

<sup>58</sup>

**SIGNIFICANCE** These results demonstrate that under delayed absorption dynamics, timing of inputs matters more than total quantity—a finding that challenges conventional drought response strategies of increased irrigation frequency. The framework offers a computationally tractable alternative to complex mechanistic models for precision agriculture optimization and is generalizable to other crops through re-parameterization.

<sup>59</sup> *Keywords:* precision agriculture, resource optimization, crop growth  
<sup>60</sup> model, genetic algorithm, cumulative stress tracking

---

<sup>61</sup> **1. Introduction**

<sup>62</sup> The agriculture sector in the United States faces significant challenges as  
<sup>63</sup> the number of farms declines and the cost of farming continues to rise [1].  
<sup>64</sup> Rising production expenses for equipment, seeds, and labor, coupled with  
<sup>65</sup> elevated interest rates and declining commodity prices, have made farming  
<sup>66</sup> increasingly expensive. To navigate this challenging landscape, farmers are  
<sup>67</sup> employing strategies such as cost management and operational optimiza-  
<sup>68</sup> tion. One promising approach is to use modeling and simulation to optimize  
<sup>69</sup> farm operations without substantial capital investment. Recent advances in  
<sup>70</sup> computational methods have enabled sophisticated digital-twin frameworks  
<sup>71</sup> for precision agriculture [2, 3], and machine learning techniques have been

72 applied to optimize sensor placement and resource delivery in agricultural  
73 systems [4, 5].

74 Mathematical modeling of crop growth has a rich history, with models  
75 ranging from simple empirical relationships to complex mechanistic simulations.  
76 Logistic growth models, first proposed by Verhulst in 1838, remain  
77 widely used due to their interpretability and ability to capture resource-  
78 limited growth dynamics [6]. More sophisticated crop models such as DSSAT  
79 [7], APSIM [8], and WOFOST [9] simulate detailed physiological processes  
80 but require extensive parameterization and may be computationally expen-  
81 sive for optimization applications. In contrast, reduced-order models that  
82 capture essential dynamics while remaining tractable for optimization have  
83 gained attention in precision agriculture [10].

84 Optimization of irrigation and fertilizer application has been studied us-  
85 ing various approaches, including linear and nonlinear programming [11],  
86 dynamic programming [12], and metaheuristic algorithms [13]. Genetic algo-  
87 rithms (GAs) are particularly well-suited for this domain because they can  
88 handle nonlinear, non-convex objective functions and do not require gradi-  
89 ent information [14]. Previous work has applied GAs to irrigation scheduling  
90 [15] and fertilizer optimization [16], but these studies often use simplified  
91 plant response models that do not capture the delayed, cumulative effects of  
92 resource application.

93 This paper presents a generalized, coupled ordinary differential equation  
94 (ODE) model for crop growth that addresses these limitations. The model  
95 captures: (1) nonlinear logistic growth with state-dependent carrying ca-  
96 pacities, (2) delayed absorption of water, fertilizer, temperature, and solar  
97 radiation inputs through finite impulse response (FIR) convolution, (3) cu-  
98 mulative stress tracking via exponential moving average (EMA) filters, and  
99 (4) coupling between vegetative and reproductive growth stages. The model  
100 is designed to enable global optimization under delayed, resource-coupled  
101 dynamics—a regime where even well-established management practices may  
102 benefit from computational refinement due to the sheer number of possible  
103 scheduling combinations.

104 We demonstrate the framework by optimizing irrigation and fertilizer  
105 strategies for corn, the most widely planted crop in the United States by  
106 acreage. Using a genetic algorithm, we search for strategies that maximize  
107 net revenue (crop value minus input costs) over a growing season. The ap-  
108 proach is validated using historical weather data from Fairfax, Iowa, a rep-  
109 resentative location in the Corn Belt.

110 **2. Generalized, coupled-ODE crop model**

111 The proposed model tracks five state variables representing key aspects  
 112 of plant development: plant height  $h$  (m), leaf area per leaf  $A$  ( $\text{m}^2$ ), num-  
 113 ber of leaves  $N$ , flower size  $c$  (number of spikelets), and fruit biomass  $P$   
 114 (kg). Each state variable follows logistic growth dynamics with time-varying  
 115 growth rates and carrying capacities that depend on environmental condi-  
 116 tions and resource availability.

117 The model receives four input signals: water from irrigation  $w$  (inches),  
 118 fertilizer application  $f$  (lbs), ambient temperature  $T$  ( $^\circ\text{C}$ ), and solar radiation  
 119  $R$  ( $\text{W/m}^2$ ). Precipitation  $S$  (inches) is added to irrigation to obtain total  
 120 water input. Temperature and radiation data are obtained from the National  
 121 Solar Radiation Database (NSRDB) [17], while precipitation data comes from  
 122 NOAA historical records [18].

123 *2.1. Delayed absorption via FIR convolution*

124 Plants do not immediately process applied nutrients; instead, there is  
 125 a physiologically-mediated delay between application and utilization. We  
 126 model this delayed absorption using finite impulse response (FIR) convolu-  
 127 tion with Gaussian kernels.

128 If cumulative nutrient uptake follows a sigmoid trajectory—with slow ini-  
 129 tial uptake due to transport lag, rapid increase once metabolic pathways acti-  
 130 vate, and eventual saturation—then instantaneous absorption rate follows a  
 131 bell-shaped curve. A Gaussian kernel is the least assumptive choice for a bell  
 132 curve, requiring only two parameters: the temporal spread  $\sigma$  (characterizing  
 133 absorption duration) and the peak delay  $\mu$ .

134 Given only the temporal spread  $\sigma$  for each nutrient type, we determine  $\mu$   
 135 such that 95% of the kernel mass lies within  $[0, 2\mu]$ . This requires solving

$$\operatorname{erf}\left(\frac{\mu}{\sigma\sqrt{2}}\right) = 0.95, \quad (1)$$

136 which yields  $\mu \approx 1.96\sigma$ . The Gaussian FIR kernel is then

$$g[k] = \frac{1}{\sqrt{2\pi\sigma^2}} \exp\left\{-\frac{1}{2}\frac{(k-\mu)^2}{\sigma^2}\right\}. \quad (2)$$

137 The FIR horizon  $L^*$  is chosen as the minimum length capturing 95% of  
 138 the kernel mass:

$$L^* = \min_L \left\{ L : \frac{\sum_{k=0}^{L-1} g[k]}{\sum_{k=0}^{K-1} g[k]} \geq 0.95 \right\} \quad (3)$$

139 where  $K$  is the simulation length in hours.

140 Different nutrients have different metabolic timescales. We use  $\sigma_w = 30$   
141 hours for water (rapid uptake),  $\sigma_f = 300$  hours for fertilizer (slow uptake re-  
142 flecting root absorption dynamics), and  $\sigma_T = \sigma_R = 30$  hours for temperature  
143 and radiation (immediate physiological effects with short memory).

#### 144 2.2. Cumulative stress tracking via EMA filtering

145 While FIR convolution captures delayed absorption, plants also accumu-  
146 late stress from sustained deviations from optimal conditions. We model this  
147 cumulative effect using exponential moving average (EMA) filters, which are  
148 equivalent to first-order infinite impulse response (IIR) systems.

149 The EMA filter with memory parameter  $\beta \in [0, 1)$  has the recursive form:

$$y[k] = (1 - \beta)x[k] + \beta y[k - 1] \quad (4)$$

150 where larger  $\beta$  values correspond to longer memory (slower response to  
151 changes). This formulation preserves constant signals ( $x[k] = c$  implies  
152  $y[k] \rightarrow c$ ) while smoothing transient fluctuations.

#### 153 2.3. Nutrient factor calculation

154 We now describe the complete transformation pipeline that converts raw  
155 input signals into nutrient factors  $\nu \in [0, 1]$  that modulate plant growth. Us-  
156 ing fertilizer as an example (the same process applies to water, temperature,  
157 and radiation):

158 **Step 1: Delayed absorption.** Convolve the raw fertilizer signal  $f[k]$   
159 with the Gaussian FIR kernel:

$$\bar{f}[k] = \sum_{n=0}^{L_f-1} g_f[n] f[k - n] \quad (5)$$

160 **Step 2: Cumulative absorption.** Compute the running sum of ab-  
161 sorbed fertilizer:

$$F[k] = \sum_{n=0}^k \bar{f}[n] \quad (6)$$

162 **Step 3: Instantaneous anomaly.** Compare actual cumulative absorp-  
163 tion to expected levels:

$$\delta_f[k] = \left| \frac{k \cdot f_{\text{typ}} - F[k]}{k \cdot f_{\text{typ}} + \epsilon} \right| \quad (7)$$

164 where  $f_{\text{typ}}$  is the typical hourly fertilizer level the plant “expects” and  $\epsilon$  is a  
165 small constant preventing division by zero.

166 **Step 4: Cumulative divergence.** Apply EMA smoothing to track  
167 sustained anomalies:

$$\Delta_f[k] = \beta_\Delta \Delta_f[k - 1] + (1 - \beta_\Delta) \delta_f[k] \quad (8)$$

168 where  $\beta_\Delta = 0.95$  provides long memory.

169 **Step 5: Nutrient factor.** Convert divergence to a stress factor via  
170 exponential decay with additional EMA smoothing:

$$\nu_f[k] = \beta_\nu \nu_f[k - 1] + (1 - \beta_\nu) \exp\{-\alpha \Delta_f[k]\} \quad (9)$$

171 where  $\alpha = 3$  ensures  $\nu \approx 0.05$  when  $\Delta = 1$  (complete divergence from  
172 expected levels), and  $\beta_\nu = 0.05$ .

173 The nutrient factor  $\nu_f[k]$  equals 1 when fertilizer application perfectly  
174 matches expected levels and decays toward 0 under sustained over- or under-  
175 application. This captures the intuition that plants are resilient to brief  
176 deviations but suffer cumulative damage from prolonged stress.

177 Figure 1 illustrates the FIR convolution and EMA smoothing operations  
178 that constitute the metabolic transformation pipeline. The left panel shows  
179 how the Gaussian FIR kernel spreads and delays input signals, while the  
180 right panel demonstrates how EMA filtering with different  $\beta$  values tracks  
181 cumulative divergence with varying memory lengths.

<sup>182</sup> 2.4. Effects of inputs on plant growth

<sup>183</sup> Different inputs affect different aspects of plant growth. Tables 1 and 2  
<sup>184</sup> summarize these relationships based on agronomic literature [19, 20, 21].

State variable	Irrigation on growth rate	Fertilizer on growth rate	Irrigation on capacity	Fertilizer on capacity
Plant height $h$	~	+	~	+
Leaf area $A$	~	+	+	+
Number of leaves $N$	~	~	~	~
Flower size $c$	~	~	+	~
Fruit biomass $P$	~	~	+	+

Table 1: Effects of irrigation and fertilizer on growth dynamics. “+” indicates positive effect, “~” indicates a negligible effect.

State variable	Temp. on growth rate	Temp. on capacity	Radiation on growth rate	Radiation on capacity
Plant height $h$	+	+	+	+
Leaf area $A$	+	+	+	+
Number of leaves $N$	~	+	~	+
Flower size $c$	-	-	-	-
Fruit biomass $P$	+	+	+	+

Table 2: Effects of temperature and solar radiation on growth dynamics. “+” indicates positive effect, “~” indicates a negligible effect, “-” indicates a negative effect. For flower size, excess heat and radiation reduce flower development, hence negative effects.

<sup>185</sup> 2.5. Growth dynamics

<sup>186</sup> Each state variable follows logistic growth with time-varying parameters  
<sup>187</sup> modulated by nutrient factors. The general form is:

$$\frac{dx}{dt} = \hat{a}_x(t) \cdot x(t) \left( 1 - \frac{x(t)}{\hat{k}_x(t)} \right) \quad (10)$$

188 where  $\hat{a}_x(t)$  is the effective growth rate and  $\hat{k}_x(t)$  is the effective carrying  
 189 capacity, both functions of the nutrient factors.

190 The effective parameters are computed as geometric means of the relevant  
 191 nutrient factors, reflecting multiplicative rather than additive effects. This  
 192 choice is motivated by the observation that growth rates compound over  
 193 time, making geometric averaging appropriate [22].

194 **Plant height** responds to fertilizer, temperature, and radiation:

$$\hat{a}_h(t) = a_h(\nu_f \nu_T \nu_R)^{1/3}, \quad \hat{k}_h(t) = k_h(\nu_f \nu_T \nu_R)^{1/3} \quad (11)$$

195 **Leaf area** additionally depends on water and is coupled to height:

$$\hat{a}_A(t) = a_A(\nu_f \nu_T \nu_R)^{1/3}, \quad \hat{k}_A(t) = k_A \left( \nu_w \nu_f \nu_T \nu_R \frac{\hat{k}_h}{k_h} \right)^{1/5} \quad (12)$$

196 **Number of leaves** depends only on temperature and radiation through  
 197 the carrying capacity:

$$\hat{a}_N(t) = a_N, \quad \hat{k}_N(t) = k_N(\nu_T \nu_R)^{1/2} \quad (13)$$

198 **Flower size** (spikelet count) exhibits inverse dependence on temperature  
 199 and radiation—excess heat and light reduce flowering:

$$\hat{a}_c(t) = a_c \left( \frac{1}{\nu_T} \frac{1}{\nu_R} \right)^{1/2}, \quad \hat{k}_c(t) = k_c \left( \nu_w \frac{1}{\nu_T} \frac{1}{\nu_R} \right)^{1/3} \quad (14)$$

200 **Fruit biomass** depends on all inputs and is coupled to vegetative growth:

$$\hat{a}_P(t) = a_P \left( \frac{1}{\nu_T} \frac{1}{\nu_R} \right)^{1/2}, \quad \hat{k}_P(t) = k_P \left( \nu_w \nu_f \nu_T \nu_R \frac{\hat{k}_h \hat{k}_A \hat{k}_c}{k_h k_A k_c} \right)^{1/7} \quad (15)$$

201 The coupling terms  $\hat{k}_h/k_h$ ,  $\hat{k}_A/k_A$ , and  $\hat{k}_c/k_c$  encode physiological depen-  
 202 dencies: taller plants with more leaf area can support larger fruit, while larger  
 203 tassels (more spikelets) may compete with ear development.

## 204 2.6. Model parameters

205 The baseline growth rates and carrying capacities are crop-specific pa-  
 206 rameters that can be estimated from field data or literature values. For corn,  
 207 we use the values in Table 3, calibrated to match typical development time-  
 208 lines where plants reach full vegetative size around 65–70 days after sowing  
 209 and grain fill completes around 125 days [23].

State	Growth rate	Carrying capacity	Initial condition	Units
Height $h$	$a_h = 0.010 \text{ hr}^{-1}$	$k_h = 3.0$	$h_0 = 0.001$	m
Leaf area $A$	$a_A = 0.0105 \text{ hr}^{-1}$	$k_A = 0.65$	$A_0 = 0.001$	$\text{m}^2$
Leaves $N$	$a_N = 0.011 \text{ hr}^{-1}$	$k_N = 20$	$N_0 = 0.001$	count
Spikelets $c$	$a_c = 0.010 \text{ hr}^{-1}$	$k_c = 1000$	$c_0 = 0.001$	count
Fruit $P$	$a_P = 0.005 \text{ hr}^{-1}$	$k_P = 0.25$	$P_0 = 0.001$	kg

Table 3: Baseline model parameters for corn. Growth rates are per hour; initial conditions are set to  $k_x/K$  where  $K \approx 2900$  is the season length in hours.

### 210 3. Simulation

211 The logistic ODE admits a closed-form solution, enabling exact time-  
 212 stepping without numerical integration error. Given state  $x(t)$  at time  $t$ , the  
 213 state at  $t + \Delta t$  is:

$$x(t + \Delta t) = \frac{\hat{k}_x(t)}{1 + \left( \frac{\hat{k}_x(t)}{x(t)} - 1 \right) \exp(-\hat{a}_x(t)\Delta t)} \quad (16)$$

214 where  $\hat{a}_x(t)$  and  $\hat{k}_x(t)$  are treated as constant over the time step. This closed-  
 215 form approach is more accurate than forward Euler integration and avoids  
 216 instability issues that can arise with explicit methods at larger time steps.

217 We simulate the growing season at hourly resolution ( $\Delta t = 1$  hour),  
 218 yielding approximately 2900 time steps for a typical corn season (late April  
 219 to early October). At each step, we: (1) update the nutrient factors based on  
 220 cumulative inputs and divergences, (2) compute effective growth rates and  
 221 carrying capacities, and (3) advance each state variable using Equation 16.

### 222 4. Optimization via genetic algorithm

223 Given the nonlinear, delay-affected dynamics of the crop model, gradient-  
 224 based optimization is challenging. The delayed effects of inputs create a  
 225 non-convex landscape with potentially many local optima. We therefore  
 226 employ a genetic algorithm (GA), a population-based metaheuristic inspired  
 227 by natural selection that can effectively explore complex search spaces [14].

228    4.1. Decision variables

229    Each candidate solution encodes a complete irrigation and fertilization  
 230    strategy as a four-dimensional vector:

$$\mathbf{u} = \begin{bmatrix} u_1 \\ u_2 \\ u_3 \\ u_4 \end{bmatrix} = \begin{bmatrix} \text{irrigation frequency (hours)} \\ \text{irrigation amount (inches)} \\ \text{fertilizer frequency (hours)} \\ \text{fertilizer amount (lbs)} \end{bmatrix} \quad (17)$$

231    The frequencies specify application intervals:  $u_1 = 168$  means irrigate  
 232    every 168 hours (weekly). The amounts specify the quantity applied at  
 233    each event. This parameterization assumes regular, periodic application—a  
 234    simplification that captures common agricultural practice while keeping the  
 235    search space tractable.

236    4.2. Objective function

237    The objective is to maximize net revenue, defined as crop value minus  
 238    input costs.

$$\text{Revenue}(\mathbf{u}) = \text{Crop Value} - \text{Input Costs} \quad (18)$$

239    The crop value depends on final plant state at harvest:

$$\text{Crop Value} = \omega_h h[K] + \omega_A A[K] + \omega_P P[K] \quad (19)$$

240    where  $K$  is the final time step and  $\omega_h$ ,  $\omega_A$ ,  $\omega_P$  are economic weights (dollars  
 241    per unit) for height, leaf area, and fruit biomass respectively.

242    The input costs accumulate over the season:

$$\text{Input Costs} = \omega_w \sum_{k=0}^K w[k] + \omega_f \sum_{k=0}^K f[k] \quad (20)$$

243    where  $\omega_w$  and  $\omega_f$  are costs per unit of irrigation and fertilizer.

244    For corn, the economic weights are derived from market prices and typical  
 245    yields (Table 4). The fruit biomass weight dominates, reflecting that grain  
 246    yield is the primary economic output.

Parameter	Value	Derivation
$\omega_w$	\$2.00/inch	Typical irrigation cost
$\omega_f$	\$0.61/lb	Weighted NPK cost
$\omega_h$	\$35/m	Silage value proxy
$\omega_A$	\$215/m <sup>2</sup>	Silage value proxy
$\omega_P$	\$4,450/kg	\$4/bushel $\times$ plant density

Table 4: Economic weights for the corn objective function. The fruit biomass weight accounts for approximately 28,350 plants per acre at \$0.157/kg.

247 *4.3. Algorithm description*

248 The GA maintains a population of  $M$  candidate solutions and iteratively  
249 improves them through selection, crossover, and mutation over  $G$  genera-  
250 tions. Algorithm 1 presents the complete procedure.

251 **Selection.** After each generation, population members are ranked by  
252 cost. The top  $P$  members survive as “parents” for the next generation. This  
253 selection ensures the best solutions are never lost.

254 **Crossover.** New “children” are created by blending two parent solutions.  
255 For each child, we randomly select two parents and compute a weighted  
256 average:

$$\mathbf{u}^{(\text{child})} = \phi \cdot \mathbf{u}^{(a)} + (1 - \phi) \cdot \mathbf{u}^{(b)} \quad (21)$$

257 where  $\phi \sim \text{Uniform}(0, 1)$  under normal operation. This crossover can produce  
258 children anywhere along the line segment connecting the parents, enabling  
259 smooth exploration of the search space.

260 **Mutation and Diversity.** To maintain population diversity and escape  
261 local optima, the remaining  $M - P - C$  population slots are filled with ran-  
262 domly generated solutions. Additionally, if the best cost stagnates (changes  
263 by less than 0.01) for 10 consecutive generations, we switch to aggressive  
264 crossover with  $\phi \sim \text{Uniform}(-1, 2)$ . This allows children to lie outside the  
265 convex hull of their parents, promoting exploration of new regions.

266 **Default Parameters.** We use  $M = 128$  members,  $P = 16$  parents,  
267  $C = 16$  children, and  $G = 100$  generations. The large population relative  
268 to generations ensures diversity for exploration while preventing premature  
269 convergence.

270    5. Case study: corn in iowa

271    We demonstrate the framework using corn, the most widely planted crop  
272    in the United States with over 90 million acres harvested annually [24].  
273    The case study uses historical weather data from Fairfax, Iowa ( $41.76^{\circ}\text{N}$ ,  
274     $91.87^{\circ}\text{W}$ ), a representative location in the Corn Belt (USDA climate zones  
275    4b–5b).

276    5.1. Scenario configuration

277    The simulation covers a typical growing season from late April to early  
278    October (approximately 2900 hours). Environmental inputs are:

- 279    • **Temperature and radiation:** Hourly data from NSRDB for Fairfax,  
280    IA. Mean temperature is  $22.8^{\circ}\text{C}$ ; mean solar radiation is  $580 \text{ W/m}^2$ .
- 281    • **Precipitation:** Daily data from NOAA, interpolated to hourly reso-  
282    lution.
- 283    • **Typical nutrient expectations:** Based on agronomic recommenda-  
284    tions [25], the model expects 28 inches of water and 355 lbs of NPK  
285    fertilizer over the season ( $w_{\text{typ}} \approx 0.01 \text{ in/hr}$ ,  $f_{\text{typ}} \approx 0.12 \text{ lb/hr}$ ).

286    Table 5 summarizes expected corn development timelines used to calibrate  
287    model parameters.

State variable	Days to maturity	Hours to maturity	Typical final value
Plant height $h$	65–70	1560–1680	2.7–3.7 m
Leaf area $A$	55–65	1320–1560	0.6–0.7 $\text{m}^2$
Number of leaves $N$	65	1560	18–20
Spikelets $c$	65–70	1560–1680	~1000
Fruit biomass $P$	125	3000	0.15–0.36 kg

Table 5: Corn development timeline and typical final values from agronomic literature [23, 26].

288    5.2. *Baseline scenario: farmer best practices under drought*

289    To establish a performance baseline, we first simulate crop growth under  
290    a drought scenario (50% of typical precipitation) using conventional farmer  
291    practices: weekly irrigation of 1 inch [27] and monthly fertilizer applications  
292    of 90 lbs [28]. These values reflect standard agronomic recommendations for  
293    corn in the Corn Belt region.

294    Figure 2 shows the environmental disturbances and control inputs over the  
295    growing season. The reduced precipitation characteristic of a drought year is  
296    clearly visible, along with the periodic irrigation and fertilizer applications.

297    Figure 3 shows the resulting plant state trajectories. Under drought conditions with conventional management, the plant reaches the following final  
298    values: height of 2.6 m (vs. 3.0 m capacity), leaf area of 0.57 m<sup>2</sup> (vs. 0.65  
299    m<sup>2</sup>), and fruit biomass of 0.22 kg (vs. 0.25 kg). The net revenue under this  
300    scenario is \$859/acre.

302        The baseline scenario demonstrates how the model captures stress ef-  
303        fects: despite regular irrigation, the mismatch between applied water and  
304        the plant's metabolic expectations under drought conditions leads to sus-  
305        tained nutrient factor depression and reduced growth potential. Detailed  
306        visualizations of the applied vs. absorbed nutrients, cumulative values, and  
307        nutrient factors are provided in the Supplementary Information.

308    5.3. Optimization configuration

309    The GA searches over the following bounds:

- 310    • Irrigation frequency: 100–700 hours (4–29 days between applications)
- 311    • Irrigation amount: 0.5–5.0 inches per application
- 312    • Fertilizer frequency: 700–2900 hours (29–121 days, i.e., 1–4 applications per season)
- 314    • Fertilizer amount: 100–500 lbs per application

315    These bounds reflect practical constraints: irrigation systems have minimum application rates, and fertilizer is typically applied in a small number of 316 large doses rather than continuously. The optimization was performed under 317 the same environmental conditions: a drought scenario with 50% of typical 318 precipitation.

320    5.4. Optimization results

321    To assess robustness of the optimization, we executed 10 independent 322 GA runs with different random seeds. Figure 4 shows the convergence of 323 all 10 runs, with each curve representing the best revenue achieved at each 324 generation. All runs converge to similar final values (within 3% of each other), 325 demonstrating that the GA reliably finds near-optimal solutions despite the 326 stochastic nature of the search.

327    The optimal strategy identified by the GA is summarized in Table 6. 328 Notably, the algorithm discovers a strategy with less frequent but larger 329 irrigation events and infrequent fertilizer applications—a pattern that mini- 330 mizes cumulative divergence from expected nutrient levels given the model’s 331 delayed absorption dynamics.

Parameter	Optimal Value	Interpretation
Irrigation frequency	1237 hours	Every $\sim$ 7 weeks
Irrigation amount	5 inches	Per application
Fertilizer frequency	803 hours	Every 33 days
Fertilizer amount	77 lbs	Per application

Table 6: Optimal irrigation and fertilization strategy identified by the GA.

332      Figure 5 shows the plant state trajectories for the best member in each of  
333      the 10 GA runs. All optimized strategies achieve substantially higher final  
334      values than the baseline farmer practices: fruit biomass ranges from 0.168–  
335      0.225 kg (vs. 0.22 kg baseline), heights reach 2.41–2.88 m (vs. 2.6 m), leaf  
336      areas reach 0.44–0.56 m<sup>2</sup> (vs. 0.57 m<sup>2</sup>), and revenues reach 778–999 \$/acre  
337      (vs. \$859/acre baseline). The consistency across runs further confirms the  
338      robustness of the optimization, and while the farmer best practice yields  
339      higher revenue than one GA run (run 2), in aggregate, the GA optimization  
340      meaningfully improved upon the baseline.

341     Table 7 provides an economic comparison between the baseline farmer  
 342     practices and the GA-optimized strategies. The best GA strategy achieves  
 343     \$999/acre net revenue compared to \$859/acre for the baseline—a 16% im-  
 344     provement. Even the worst members in each GA run’s final population out-  
 345     perform the baseline, providing a sanity check that random strategies are not  
 346     viable (see Supplementary Information).

Metric	GA-Optimized	Baseline
Final fruit biomass	0.22 kg	0.22 kg
Final height	2.8 m	2.6 m
Final leaf area	0.60 m <sup>2</sup>	0.57 m <sup>2</sup>
Total irrigation	15 inches	18 inches
Total fertilizer	307 lbs	450 lbs
Crop value	\$1218	\$1171
Input costs	\$219	\$312
<b>Revenue</b>	<b>\$999</b>	<b>\$859</b>

Table 7: Economic comparison of GA-optimized versus baseline farmer strategies. The optimized strategy achieves 16% higher net revenue through both increased crop value and dramatically reduced irrigation costs.

## 347     6. Discussion

### 348     6.1. Interpretation of results

349     The GA-optimized strategy differs from conventional wisdom in several  
 350     notable ways. The algorithm discovers that less frequent but larger irrigation  
 351     events, combined with reduced total fertilizer input, can outperform conven-  
 352     tional uniform application schedules. This counterintuitive result emerges  
 353     from the model’s delayed absorption dynamics: under drought conditions,  
 354     the plant’s metabolic expectations are calibrated to typical water availabil-  
 355     ity. The GA discovers that strategically-timed resource inputs better main-  
 356     tain alignment with metabolic expectations than aggressive compensation  
 357     for drought through frequent, uniform applications.

358     The consistency across 10 independent GA runs provides confidence that  
 359     the optimization reliably identifies high-performing regions of the strategy  
 360     space. While individual runs converge to somewhat different local optima  
 361     (with revenues ranging from \$778 to \$983 per acre), 9 of 10 runs outperform

362 the baseline farmer practices, demonstrating the robustness of the optimization  
363 approach. The sanity check showing that even the worst members in  
364 each final population generally outperform baseline practices confirms that  
365 the GA successfully eliminates poor candidates.

366 The 16% revenue improvement (\$999 vs. \$859 per acre) demonstrates sub-  
367 substantial potential value from model-based optimization. This improvement  
368 comes from two sources: (1) increased crop value due to better-aligned nu-  
369 trient delivery, and (2) reduced input costs. The result suggests that conven-  
370 tional wisdom about drought response—applying more water to compensate—  
371 may be suboptimal when plant physiology involves delayed, cumulative-effect  
372 dynamics.

### 373 6.2. Parameter estimation in practice

374 The framework requires crop-specific parameters: growth rates, carrying  
375 capacities, metabolic timescales, and typical nutrient expectations. Several  
376 approaches could estimate these from data:

- 377 • **Growth curves:** Time-series imagery from field cameras or drones,  
378 processed with computer vision, could provide height and leaf area  
379 trajectories for fitting  $a_x$  and  $k_x$  parameters.
- 380 • **Metabolic timescales:** The temporal spreads  $\sigma$  could be estimated  
381 from controlled experiments varying input timing, or inferred from  
382 physiological literature on nutrient uptake rates.
- 383 • **Typical expectations:** Regional agronomic recommendations pro-  
384 vide baseline values for  $w_{typ}$ ,  $f_{typ}$ ,  $T_{typ}$ , and  $R_{typ}$ .

385 Physics-informed neural networks (PINNs) could jointly fit model param-  
386 eters and approximate unknown functional forms in the dynamics, potentially  
387 relaxing some of the structural assumptions in Section 2.

### 388 6.3. Limitations and extensions

389 Several model limitations suggest directions for future work:

390 **Growth model.** The logistic equation assumes symmetric growth around  
391 the inflection point. Richards growth [29] generalizes this with a shape pa-  
392 rameter  $\nu$ :

$$\frac{dx}{dt} = a_x x \left[ 1 - \left( \frac{x}{k_x} \right)^\nu \right] \quad (22)$$

393 where  $\nu > 1$  produces steeper early growth (common in vegetative stages)  
394 and  $\nu < 1$  produces steeper late growth.

395 **Absorption kernels.** Gaussian kernels are symmetric, but physiological  
396 absorption often exhibits fast activation followed by slow decay. Log-normal  
397 or Gamma kernels could better capture this asymmetry.

398 **Saturation.** The current model does not explicitly limit nutrient uptake—  
399 all applied inputs eventually affect the plant. In reality, excess application  
400 may be lost to runoff or leaching. Saturating nonlinearities in the absorption  
401 pathway would provide a more realistic response to over-application.

402 **Spatial heterogeneity.** The model treats a single representative plant.  
403 Field-scale optimization would need to account for spatial variation in soil  
404 properties, microclimate, and plant density.

405 **Stochastic weather.** The case study uses historical weather data. Ro-  
406 bust optimization under weather uncertainty, or adaptive strategies that re-  
407 spond to observed conditions, could improve real-world performance.

## 408 7. Conclusion

409 This paper presented a coupled ODE model for crop growth that cap-  
410 tures delayed nutrient absorption via FIR convolution and cumulative stress  
411 effects via EMA filtering. The model’s time-varying growth rates and carry-  
412 ing capacities encode the intuition that plant development depends not just  
413 on current conditions but on the history of resource availability relative to  
414 physiological expectations.

415 Applied to corn optimization in Iowa under drought conditions, a ge-  
416 netic algorithm discovered irrigation and fertilizer strategies that achieve  
417 16% higher net revenue than conventional farmer practices (\$999 vs. \$859  
418 per acre). This improvement emerges from the model’s delayed absorption  
419 dynamics: strategic timing of inputs that aligns with metabolic expectations  
420 outperforms uniform application schedules. The consistency across 10 inde-  
421 pendent optimization runs, with 9 of 10 outperforming the baseline, confirms  
422 the robustness of these findings.

423 The framework is generalizable to other crops through re-parameterization  
424 and offers a computationally tractable approach to input optimization. Fu-  
425 ture work will extend the model to handle weather uncertainty, incorporate  
426 spatial heterogeneity, and validate predictions against field trial data.

<sup>427</sup> **8. Supplementary information**

<sup>428</sup> This supplementary section provides additional visualizations of the base-  
<sup>429</sup> line scenario (farmer best practices under drought) and the GA optimization  
<sup>430</sup> results.

<sup>431</sup> *S1. Detailed baseline scenario analysis*

<sup>432</sup> Figure 6 shows the applied versus absorbed nutrients under the baseline  
<sup>433</sup> scenario. The delayed absorption via FIR convolution is clearly visible: the  
<sup>434</sup> absorbed signals (smoothed curves) lag behind the applied inputs and exhibit  
<sup>435</sup> the characteristic spreading effect of the Gaussian kernels.

<sup>436</sup> Figure 7 shows the cumulative absorbed nutrients compared to expected  
<sup>437</sup> (typical) levels. Under drought conditions, actual water absorption falls pro-  
<sup>438</sup> gressively below expectations, while fertilizer, temperature, and radiation  
<sup>439</sup> track more closely to typical values.

<sup>440</sup> Figure 8 shows the instantaneous divergence from expected cumulative  
<sup>441</sup> levels. These divergences, after EMA smoothing, determine the nutrient  
<sup>442</sup> factors that modulate plant growth.

<sup>443</sup> Figure 9 shows the resulting nutrient factors. The water factor  $\nu_w$  declines  
<sup>444</sup> throughout the season as drought stress accumulates, reaching approximately  
<sup>445</sup> 0.6 by harvest. This reduced water factor is the primary driver of the sub-  
<sup>446</sup> optimal crop growth observed in the baseline scenario.

447 *S2. GA optimization: worst-case analysis*

448 As a sanity check, Figure 10 shows the plant state trajectories for the  
449 *worst* member in each GA run’s final population. Even these subopti-  
450 mal strategies—the least fit survivors after 100 generations of evolution—  
451 outperform the baseline farmer practices. This confirms that: (1) the GA  
452 successfully eliminates poor strategies, and (2) random or arbitrary irri-  
453 gation/fertilization schedules cannot match even the worst optimized ap-  
454 proaches.

455 **9. Acknowledgements**

456 This work has been partially supported by the UC Berkeley College of  
457 Engineering and the USDA AI Institute for Next Generation Food Systems  
458 (AIFS), USDA award number 2020-67021-32855.

459 **Declarations**

460 **Competing Interests** The authors declare that they have no known com-  
461 peting financial interests or personal relationships that could have appeared  
462 to influence the work reported in this paper.

463 **Code availability** The source code used for this study is archived on Zen-  
464 odo at <https://doi.org/10.5281/zenodo.18204023>.

466 **Declaration of generative AI and AI-assisted technologies in the  
467 manuscript preparation process** During the preparation of this work the  
468 authors used ChatGPT and Claude Code in order to generate some portions  
469 of the code base, though no underlying theory, and refine the original drafts of  
470 the paper. After using this tool/service, the authors reviewed and edited the  
471 content as needed and take full responsibility for the content of the published  
472 article.

474 **References**

- 475 [1] Economic Research Service, Farm income and wealth statistics, US  
476 Department of Agriculture (2024).  
477 URL [https://www.ers.usda.gov/data-products/  
478 farm-income-and-wealth-statistics/](https://www.ers.usda.gov/data-products/farm-income-and-wealth-statistics/)
- 479 [2] T. I. Zohdi, A machine-learning enabled digital-twin framework for  
480 next generation precision agriculture and forestry, Computer Meth-  
481 ods in Applied Mechanics and Engineering 428 (2024) 117250. doi:  
482 [10.1016/j.cma.2024.117250](https://doi.org/10.1016/j.cma.2024.117250).
- 483 [3] E. Mengi, C. J. Becker, M. Sedky, S. Yu, T. I. Zohdi, A digital-twin  
484 and rapid optimization framework for optical design of indoor farming  
485 systems, Computational Mechanics 72 (2023) 953–970. doi:[10.1007/  
486 s00466-023-02421-9](https://doi.org/10.1007/s00466-023-02421-9).

- 487 [4] P. Goodrich, O. Betancourt, A. Arias, T. I. Zohdi, Placement and drone  
488 flight path mapping of agricultural soil sensors using machine learning,  
489 Computers and Electronics in Agriculture 198 (2022) 107591. doi:10.  
490 1016/j.compag.2022.107591.
- 491 [5] I. Tagkopoulos, S. F. Brown, X. Liu, Q. Zhao, T. I. Zohdi, J. M. Earles,  
492 N. Nitin, D. E. Runcie, D. G. Lemay, A. D. Smith, P. C. Ronald, H. Feng,  
493 G. D. Youtsey, Special report: AI institute for next generation food  
494 systems (AIFS), Computers and Electronics in Agriculture 196 (2022)  
495 106819. doi:10.1016/j.compag.2022.106819.
- 496 [6] P.-F. Verhulst, Notice sur la loi que la population suit dans son accroissement,  
497 Correspondance mathématique et physique 10 (1838) 113–126.  
498 doi:10.1007/BF02309004.
- 499 [7] J. W. Jones, G. Hoogenboom, C. H. Porter, K. J. Boote, W. D. Batchelor,  
500 L. Hunt, P. W. Wilkens, U. Singh, A. J. Gijsman, J. T. Ritchie, The  
501 dssat cropping system model, European Journal of Agronomy 18 (3-4)  
502 (2003) 235–265. doi:10.1016/S1161-0301(02)00107-7.
- 503 [8] D. P. Holzworth, N. I. Huth, P. G. deVoil, E. J. Zurcher, N. I. Hermann,  
504 G. McLean, K. Chenu, E. J. van Oosterom, V. Snow, C. Murphy,  
505 et al., Apsim—evolution towards a new generation of agricultural systems  
506 simulation, Environmental Modelling & Software 62 (2014) 327–350.  
507 doi:10.1016/j.envsoft.2014.07.009.
- 508 [9] C. Van Diepen, J. Wolf, H. Van Keulen, C. Rappoldt, Wofost: a simu-  
509 lation model of crop production, Soil Use and Management 5 (1) (1989)  
510 16–24. doi:10.1111/j.1475-2743.1989.tb00755.x.
- 511 [10] R. Gebbers, V. I. Adamchuk, Precision agriculture and food security,  
512 Science 327 (5967) (2010) 828–831. doi:10.1126/science.1183899.
- 513 [11] A. Singh, An overview of the optimization modelling applications, Jour-  
514 nal of Hydrology 466–467 (2012) 167–182. doi:10.1016/j.jhydrol.  
515 2012.08.004.
- 516 [12] J. E. Epperson, J. E. Hook, Y. R. Mustafa, Dynamic program-  
517 ming for improving irrigation scheduling strategies of maize,  
518 Agricultural Systems 42 (1) (1993) 85–101, applications of

- 519        Dynamic Optimization Techniques to Agricultural Problems.  
520        doi:[https://doi.org/10.1016/0308-521X\(93\)90070-I](https://doi.org/10.1016/0308-521X(93)90070-I).  
521        URL <https://www.sciencedirect.com/science/article/pii/0308521X9390070I>
- 523 [13] W. Ding, C. Lin, Application of genetic algorithms to agriculture: a  
524        review, Computers and Electronics in Agriculture 175 (2020) 105524.  
525        doi:[10.1016/j.compag.2020.105524](https://doi.org/10.1016/j.compag.2020.105524).
- 526 [14] D. E. Goldberg, Genetic Algorithms in Search, Optimization, and Ma-  
527        chine Learning, Addison-Wesley, Reading, MA, 1989.
- 528 [15] R. Wardlaw, K. Bhaktikul, Application of genetic algorithms for irriga-  
529        tion water scheduling, Irrigation and Drainage 53 (4) (2004) 397–414.  
530        doi:[10.1002/ird.121](https://doi.org/10.1002/ird.121).
- 531 [16] Z. Yu, W. Fu, Optimization of nitrogen fertilization strategies for drip  
532        irrigation of cotton in large fields by dssat combined with a genetic  
533        algorithm, Applied Sciences 15 (7) (2025) 3580.
- 534 [17] M. Sengupta, Y. Xie, A. Lopez, A. Habte, G. MacLaurin, J. Shelby, The  
535        national solar radiation data base (nsrdb), Renewable and Sustainable  
536        Energy Reviews 89 (2018) 51–60. doi:[10.1016/j.rser.2018.03.003](https://doi.org/10.1016/j.rser.2018.03.003).
- 537 [18] National Oceanic and Atmospheric Administration, Climate data online  
538        (2024).  
539        URL <https://www.ncdc.noaa.gov/cdo-web/>
- 540 [19] J. E. Sawyer, E. D. Nafziger, G. W. Randall, L. G. Bundy, G. W.  
541        Rehm, B. C. Joern, Nitrogen management for corn production, Iowa  
542        State University Extension Publication PM 1714 (2006).
- 543 [20] J. O. Payero, D. D. Tarkalson, S. Irmak, D. R. Davison, J. L. Petersen,  
544        Effect of irrigation amounts applied with subsurface drip irrigation on  
545        corn evapotranspiration, yield, water use efficiency, and dry matter pro-  
546        duction in a semiarid climate, Agricultural Water Management 95 (8)  
547        (2008) 895–908. doi:[10.1016/j.agwat.2008.02.015](https://doi.org/10.1016/j.agwat.2008.02.015).
- 548 [21] B. Sánchez, A. Rasmussen, J. R. Porter, Temperatures and the growth  
549        and development of maize and rice: a review, Global Change Biology  
550        20 (2) (2014) 408–417. doi:[10.1111/gcb.12389](https://doi.org/10.1111/gcb.12389).

- 551 [22] R. C. Lewontin, D. Cohen, On population growth in a randomly varying  
552 environment, *Proceedings of the National Academy of Sciences* 62 (4)  
553 (1969) 1056–1060. doi:10.1073/pnas.62.4.1056.
- 554 [23] L. J. Abendroth, R. W. Elmore, M. J. Boyer, S. K. Marlay, In corn  
555 growth and development, Iowa State University Extension Publication  
556 PMR 1009 (2011).
- 557 [24] US Department of Agriculture, 2023 acreage data as of august 9, 2023  
558 (2023).
- 559 [25] J. Sawyer, E. Nafziger, G. Randall, L. Bundy, G. Rehm, B. Joern, Con-  
560 cepts and rational for regional nitrogen rate guidelines for corn, Univer-  
561 sity Extension Iowa State University Ames (2006).
- 562 [26] F. Schierbaum, Book reviews: Corn: Chemistry and technology, 2nd  
563 edition. by pamela j. white and lawrence a. johnson (editors), Starch-  
564 starke - STARCH 56 (2004) 263–264. doi:10.1002/star.200490027.
- 565 [27] W. L. Kranz, S. Irmak, S. J. van Donk, C. D. Yonts, D. L. Martin, Irri-  
566 gation management for corn, Tech. Rep. G1850, University of Nebraska–  
567 Lincoln Extension (2008).  
568 URL <https://extensionpubs.unl.edu/publication/g1850/>
- 569 [28] B. Davies, J. A. Coulter, P. H. Pagliari, Timing and rate of nitrogen  
570 fertilization influence maize yield and nitrogen use efficiency, *PLOS ONE*  
571 15 (5) (2020) e0233674. doi:10.1371/journal.pone.0233674.
- 572 [29] F. J. Richards, A flexible growth function for empirical use, *Journal of*  
573 *Experimental Botany* 10 (2) (1959) 290–301. doi:10.1093/jxb/10.2.  
574 290.

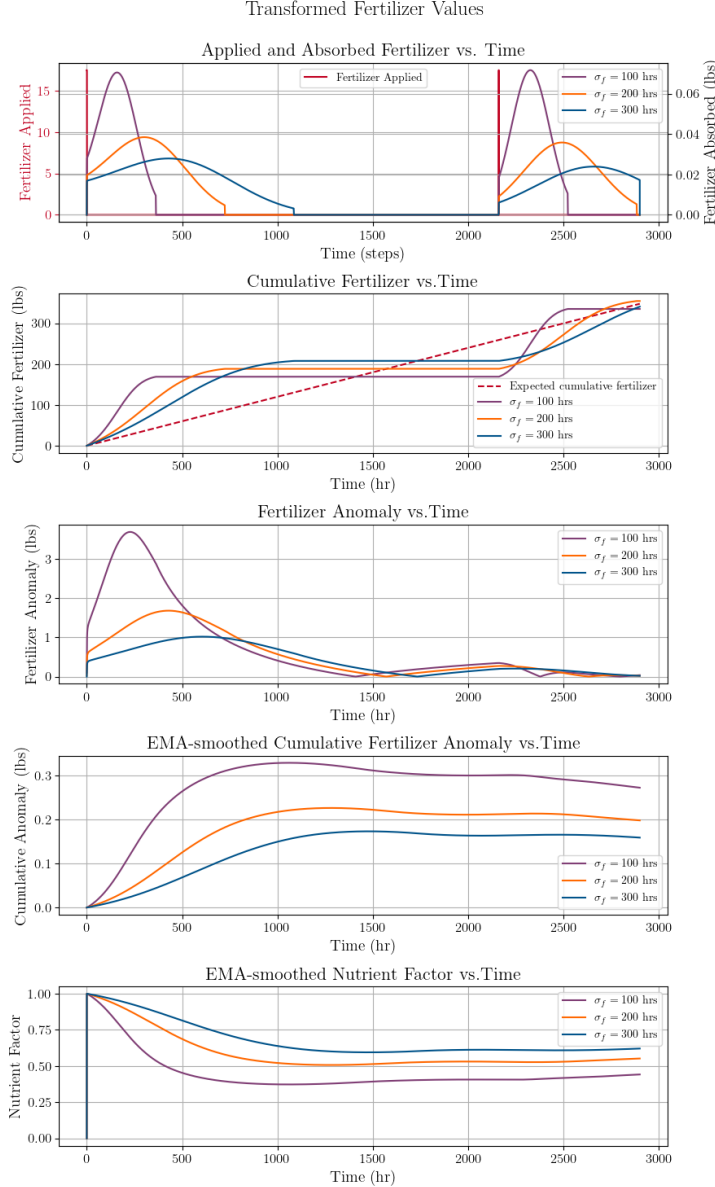


Figure 1: Illustration of the metabolic transformation pipeline. Panel 1: Gaussian FIR kernels with different temporal spreads  $\sigma$  demonstrate how water ( $\sigma_w = 30$  hr) is absorbed more rapidly than fertilizer ( $\sigma_f = 300$  hr). Panel 4: EMA filters with different memory parameters  $\beta$  show how cumulative divergence tracking responds to sustained anomalies, with larger  $\beta$  providing longer memory of past stress events.

---

**Algorithm 1** Genetic Algorithm for Input Optimization

---

- 1: **Input:** Population size  $M$ , parents  $P$ , children  $C$ , generations  $G$ , bounds  $[\mathbf{u}_{\min}, \mathbf{u}_{\max}]$
- 2: **Output:** Best solution  $\mathbf{u}^*$
- 3:
- 4: Initialize population  $\{\mathbf{u}^{(1)}, \dots, \mathbf{u}^{(M)}\}$  uniformly in bounds
- 5: Evaluate Cost( $\mathbf{u}^{(i)}$ ) for all  $i$  via full-season simulation
- 6: Sort population by cost (ascending)
- 7: stagnation  $\leftarrow 0$
- 8:
- 9: **for**  $g = 1$  to  $G$  **do**
- 10:   **Selection:** Keep top  $P$  members as parents
- 11:
- 12:   **Crossover:** Generate  $C$  children
- 13:   **for**  $j = 1$  to  $C$  **do**
- 14:     Select parents  $\mathbf{u}^{(a)}, \mathbf{u}^{(b)}$  randomly from top  $P$
- 15:     **if** stagnation  $< 10$  **then**
- 16:        $\phi \sim \text{Uniform}(0, 1)$
- 17:     **else**
- 18:        $\phi \sim \text{Uniform}(-1, 2)$  ▷ Aggressive exploration
- 19:     **end if**
- 20:      $\mathbf{u}^{(\text{child})} \leftarrow \phi \cdot \mathbf{u}^{(a)} + (1 - \phi) \cdot \mathbf{u}^{(b)}$
- 21:     Clip to bounds
- 22:   **end for**
- 23:
- 24:   **Fill remaining:** Generate  $M - P - C$  random members
- 25:   Evaluate costs for new members
- 26:   Sort population by cost
- 27:
- 28:   **Stagnation check:**
- 29:   **if**  $|\text{Cost}^{(g)} - \text{Cost}^{(g-1)}| < 0.01$  **then**
- 30:     stagnation  $\leftarrow$  stagnation + 1
- 31:   **else**
- 32:     stagnation  $\leftarrow 0$
- 33:   **end if**
- 34: **end for**
- 35:
- 36: **return**  $\mathbf{u}^{(1)}$  (best member)

---

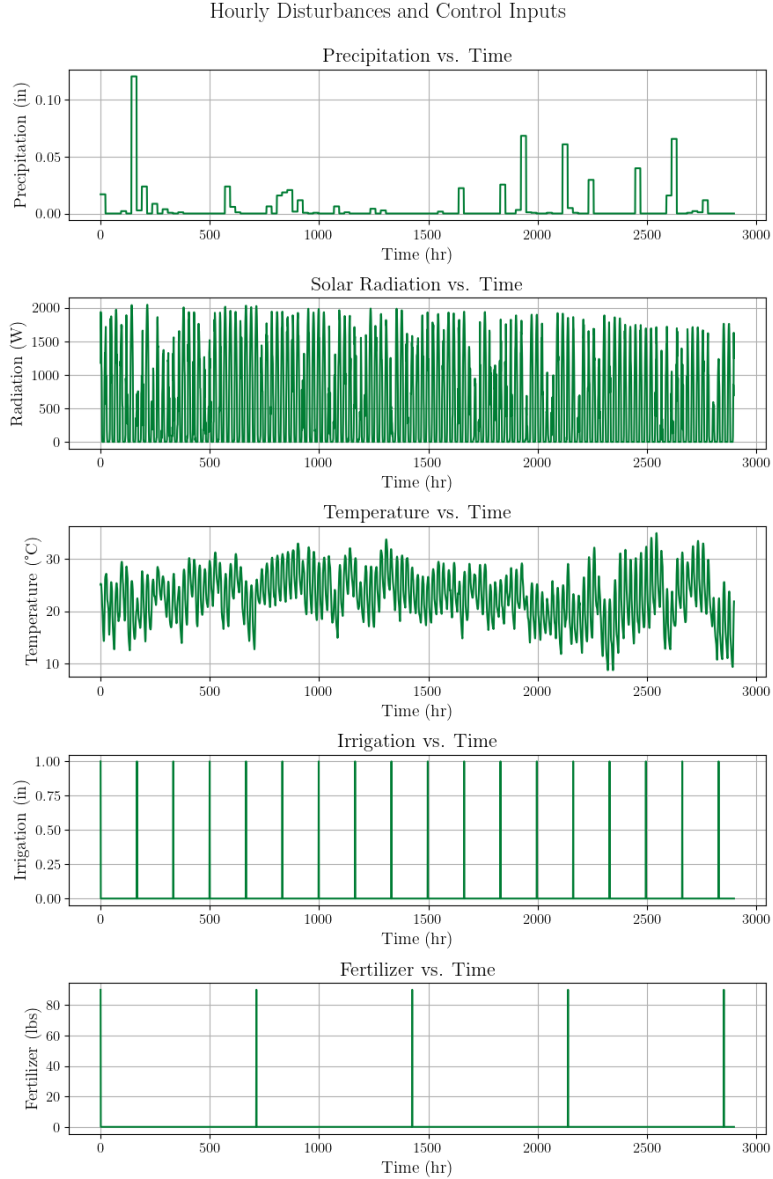


Figure 2: Environmental disturbances and control inputs for the baseline scenario. Top three panels show hourly precipitation (reduced to 50% of normal), solar radiation, and temperature from historical Iowa data. Bottom two panels show the farmer's irrigation (weekly, 1 inch) and fertilizer (monthly, 90 lbs) application strategy.

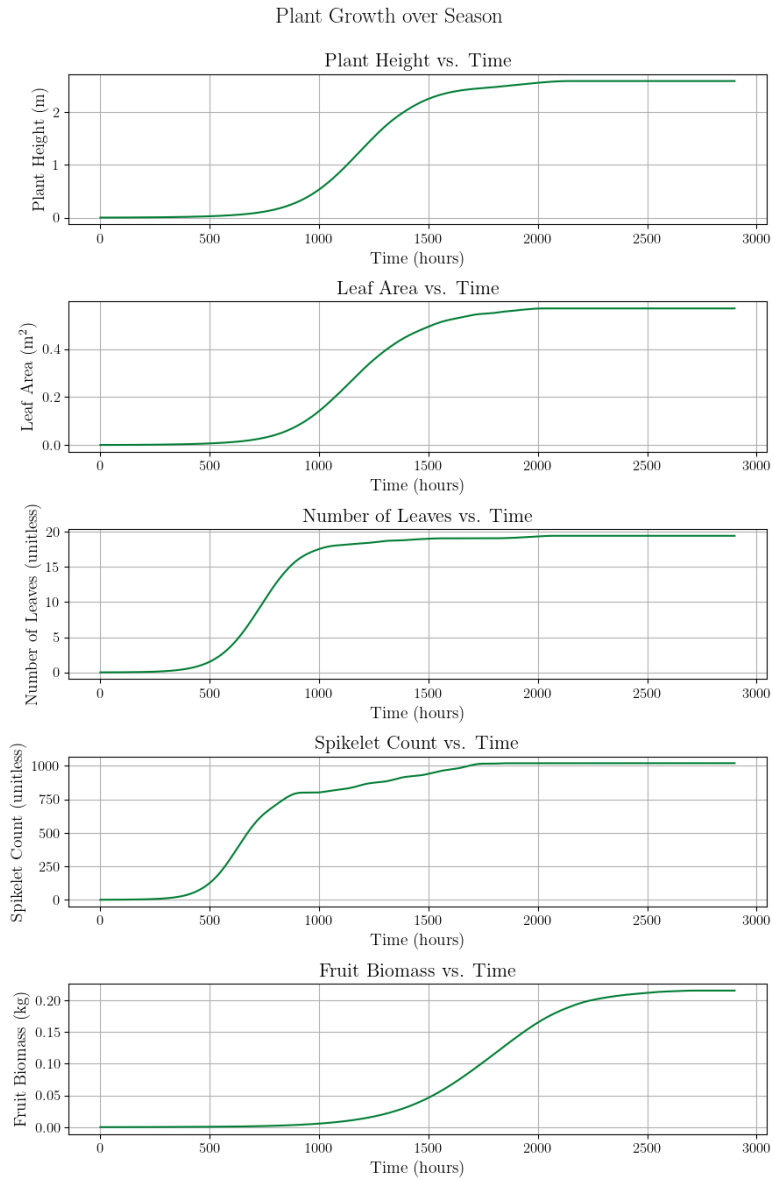


Figure 3: Plant state variable trajectories under the baseline scenario (farmer best practices during drought). All state variables reach suboptimal final values due to cumulative water stress. This strategy yields \$859/acre in revenue.

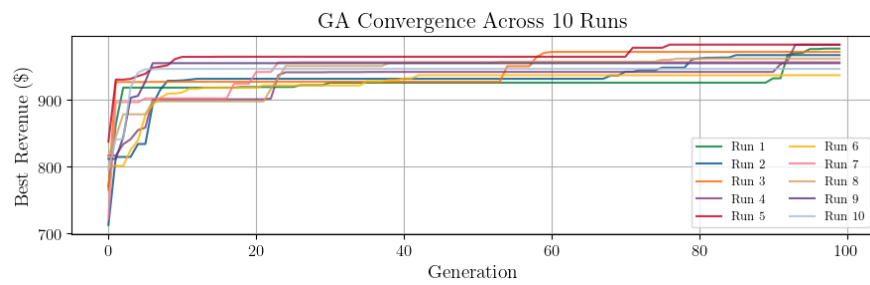


Figure 4: GA convergence across 10 independent runs. Each curve shows the best revenue at each generation. All runs exhibit rapid improvement in early generations followed by convergence to near-optimal solutions. The consistency across runs demonstrates algorithm robustness.

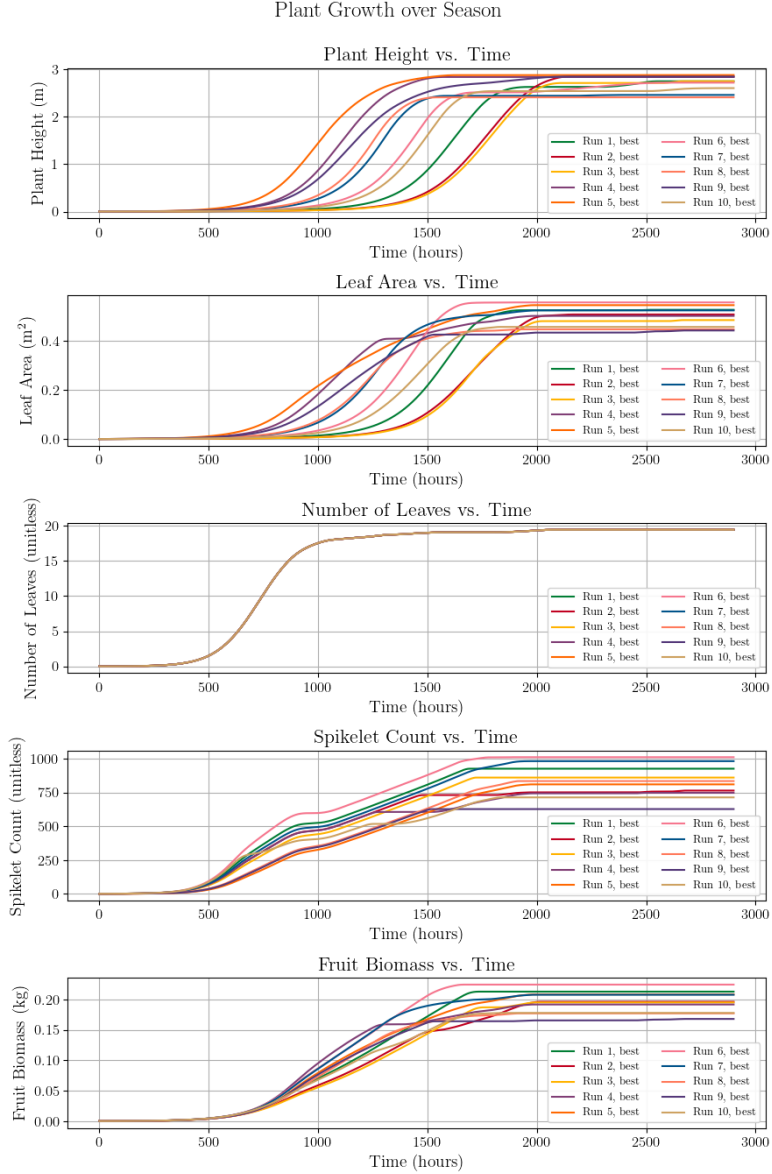


Figure 5: Plant state variable trajectories for the best member from each of the 10 independent GA runs. All optimized strategies achieve similar, near-optimal growth trajectories, and 9 of 10 runs substantially outperform the baseline farmer practices (Figure 3). The tight clustering of trajectories demonstrates that different GA runs converge to similar optimal strategies.

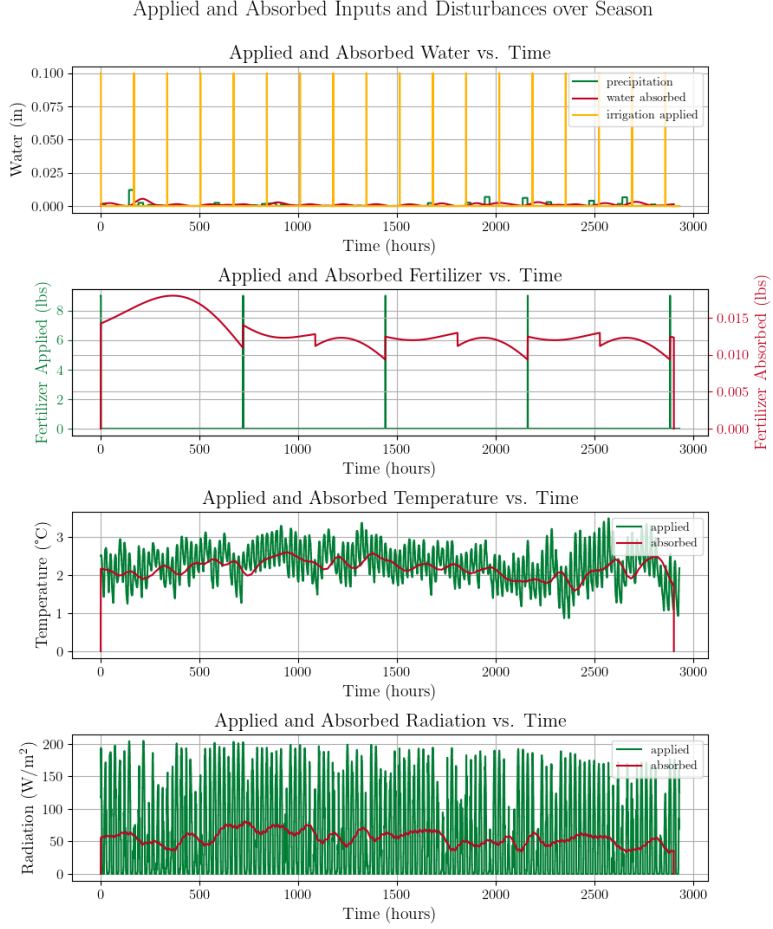


Figure 6: Applied versus absorbed nutrients under the baseline farmer strategy. The delayed absorption dynamics are evident in the lag between applied inputs and the smoothed absorbed signals. Water absorption ( $\sigma_w = 30$  hr) responds more quickly than fertilizer absorption ( $\sigma_f = 300$  hr).

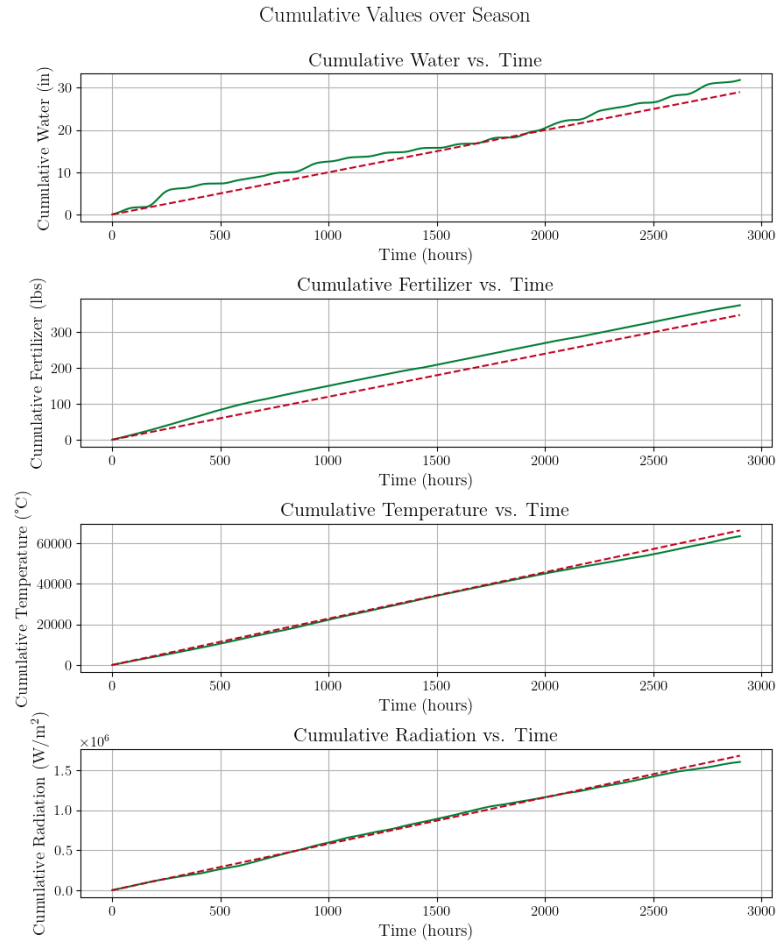


Figure 7: Cumulative absorbed nutrients (solid) versus expected levels (dashed red). The growing gap between actual and expected water absorption reflects the drought stress accumulating over the season. Fertilizer applications maintain closer alignment with expectations.

Differences between Actual and Typical Cumulative Values

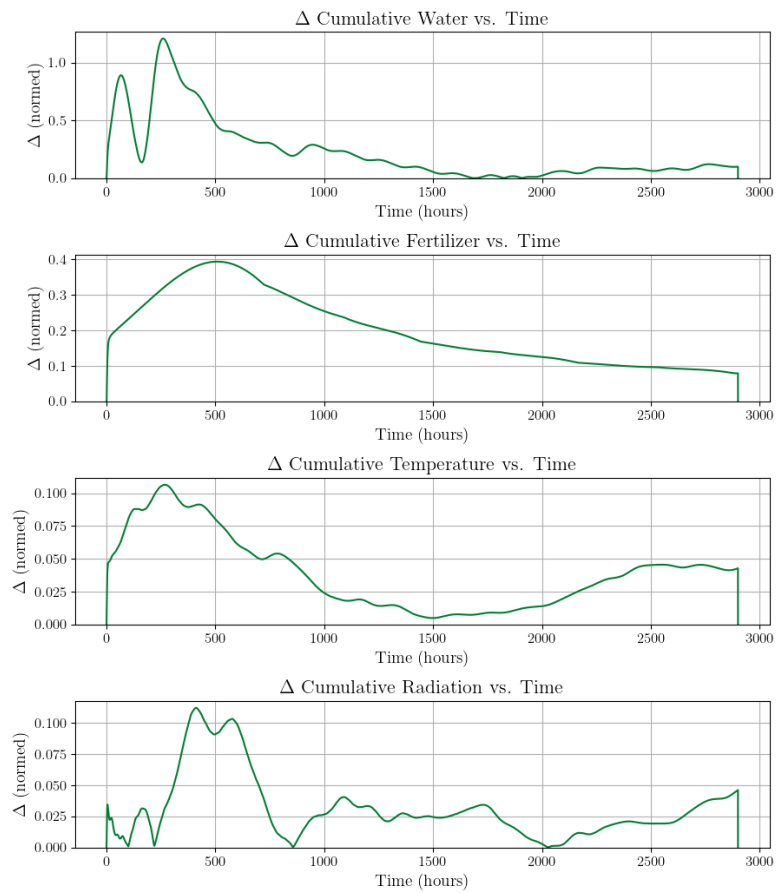


Figure 8: Instantaneous divergence from expected cumulative nutrient levels. Higher divergence indicates greater stress. The water divergence grows throughout the season due to cumulative drought effects.

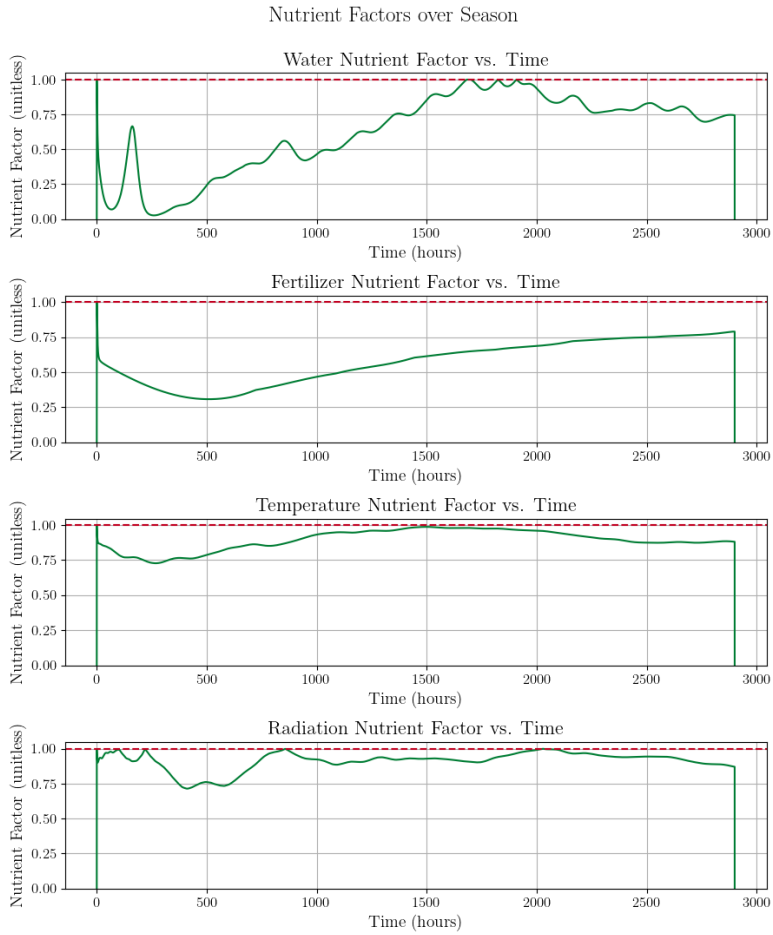


Figure 9: Nutrient factor evolution under the baseline scenario. The water factor  $\nu_w$  declines due to cumulative drought stress, while fertilizer, temperature, and radiation factors remain closer to 1.0 (no stress). The declining  $\nu_w$  reduces effective growth rates and carrying capacities throughout the season.

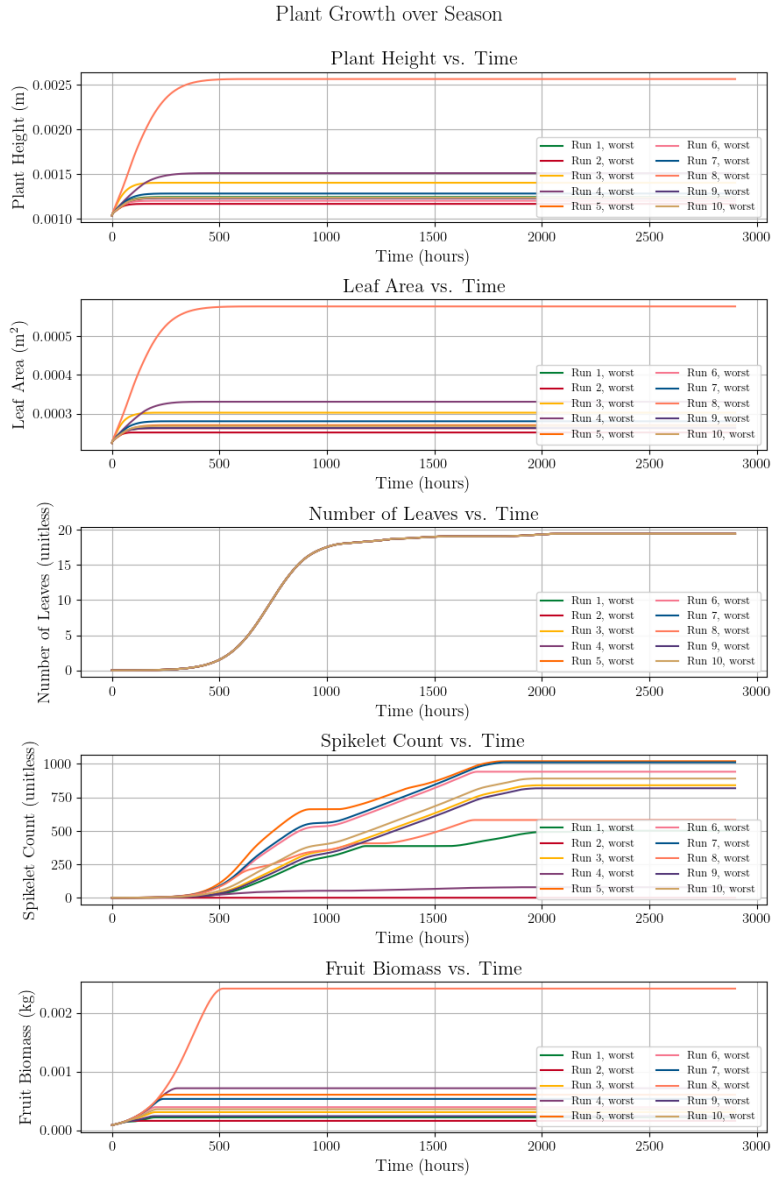


Figure 10: Plant state variable trajectories for the worst member from each GA run's final population. Even these suboptimal strategies outperform baseline farmer practices (compare to Figure 3), demonstrating that the GA successfully identifies the high-performing region of the strategy space and that random strategies are not competitive.